JOURNAL OF MOLECULAR SPECTROSCOPY 171, 189–199 (1995)

The Microwave Spectrum and Structure of CH_3NO_2–H_2O [1]

F. J. LOVAS, N. ZOBOV,[2] G. T. FRASER, AND R. D. SUENRAM

Molecular Physics Division, National Institute of Standards and Technology, Gaithersburg, Maryland 20899

The microwave spectrum of the nitromethane-water complex (CH_3NO_2–H_2O) has been studied with a pulsed-beam Fourier-transform Fabry–Perot-cavity spectrometer. Both *a*-type and *b*-type transitions were observed for the *A* state of the complex with the *b*-type transition being more intense by a factor of 2. Critical to the rotational assignments were well resolved ^{14}N nuclear electric quadrupole transitions, and the incorporation of the pulsed nozzle in one of the mirrors which provided a beam coaxial with the cavity axis to attain linewidths of about 2 kHz (full-width at half maximum—FWHM). To provide additional structural information, the spectra of the HDO, D_2O, and CD_3NO_2 substituents were assigned. The molecular structure derived from the moments of inertia has a center of mass separation of 3.506(7) Å. The moments of inertia can not distinguish between two possible forms of the complex, one with the dipole moment vectors aligned and the other with them antialigned. Measurement of the dipole moment components, $\mu_a = 4.15(4) \times 10^{-30}$ C·m ($\mu_a = 1.243(11)$ D) and $\mu_b = 5.96(4) \times 10^{30}$ C·m ($\mu_b = 1.706(12)$ D), resolves this difficulty and shows that the dipole moment vectors are antialigned. The molecular complex is quite strongly bound with a harmonic pseudodiatomic stretching force constant, $k_s = 9.30$ N/m, and hydrogen bond lengths of approximately 2.1 Å between the water O atom and a CH_3 H atom, and between a water H atom and an oxygen atom of NO_2. One standard deviation uncertainty is shown in parentheses for each experimental value reported.

I. INTRODUCTION

The stimulus for the study of the nitromethane-water complex derives from the theoretical work of Melius (*1*, *2*), which indicates that water exerts a strong catalytic effect in reducing the barrier to the decomposition of nitramines. Examples are presented for the reactions of nitramine and nitromethane in which, according to Melius (*2*), "water provides a concerted, cyclic reaction pathway for reduction of the nitro group." The transition state, depicted in Fig. 1(b) of Ref. (*2*), shows a reduction in the barriers by 113 kJ mole^{-1} (27 kcal mole^{-1}) in the water catalyzed conversion of nitromethane to the *aci* form:

$$CH_3NO_2 + H_2O \rightarrow CH_2N(O)OH + H_2O. \quad (1)$$

We have studied a number of molecular complexes in which the transition state configuration is mimicked by the geometry of the van der Waals complex, strongly suggesting for a number of reactions that the minimum energy configuration of the complexes lies along the reaction coordinate. Examples studied include the complexes of

[1] Certain commercial material and equipment are identified in the paper in order to specify the experimental procedure. In no case does such identification imply recommendation or endorsements by the National Institute of Standards and Technology, nor does it imply that the material or equipment identified is necessarily the best available for the purpose.

[2] Guest worker, 1993-1994; permanent address: Institute of Applied Physics, Nizhny, Novgorod, Russia.

0022-2852/95 $6.00

ozone–ethylene (*3*), ozone–acetylene (*4*), and ketene–ethylene (*5*). The success of these prior studies motivated us to compare the structure of the nitromethane–water complex with the proposed cyclic transition-state geometry of Melius (*2*).

II. EXPERIMENTAL PROCEDURE

Measurements were made between 8 and 18 GHz using a pulsed-beam Fabry–Perot-cavity Fourier-transform microwave spectrometer (*6, 7*) of the Balle–Flygare type (*8*). In the initial experiments, a dual-inlet pulsed solenoid valve (*4*) was used to deliver a supersonic molecular beam from separate samples of about 0.5–1 vol% CH_3NO_2 and H_2O entrained in Ne carrier gas at a total nozzle backing pressure of 150 kPa (1.5 atm) to the center of a Fabry–Perot cavity. Molecular-beam pulses from a 0.5-mm orifice with 200–400 μsec duration were employed with repetition rates up to 35 Hz with the nozzle perpendicular to the cavity axis. The molecular complex was polarized by a short microwave pulse when the microwave frequency was near resonant ($\Delta\nu < 400$ kHz) with a rotational transition of the complex. The free induction decay signal from the cavity was digitized in 0.5-μsec increments for 400 channels, and then Fourier transformed to obtain the power spectrum with a resolution element of 5.0 kHz/point. To obtain preliminary rotational state assignments, Stark fields were applied to the molecular beam by two parallel plates (26 × 26 cm) separated by ~26 cm by using voltages up to +2 and −2 kV on each plate. The analysis was complicated by the partially resolved ^{14}N nuclear quadrupole hyperfine structure. In the later stages of the experiment a new spectrometer was employed in which a molecular beam coaxial with the cavity axis was used to obtain higher resolution and enhanced sensitivity. The hyperfine patterns could now be fully resolved, and were used in identifying the J and K quantum numbers of the transitions. The configuration on the new spectrometer will be briefly described below.

The mechanical configuration was essential the same as that previously described (*6*) with the exception that the nozzle is located near the center of one of the mirrors with a 1 mm dia. × 6 mm cylindrical beam exit channel in the mirror. Grabow and Stahl (*9*) describe the first implementation of a pulsed nozzle coaxial with the mirror axis by placing a nozzle in one of the mirrors as close to the center as possible; we have essentially duplicated this modification, although in our case both mirrors are enclosed in the vacuum chamber and both are movable via motorized micrometers. The coaxial configuration provides a narrower linewidth, ~6 kHz (FWHM), and improved sensitivity due to the five- to sixfold increase of the interaction time in the cavity.

In addition to the new nozzle configuration, a number of changes have been made in the microwave and electronic components. A 10-MHz reference signal is used to synchronize the synthesizer, pulse sequencer, and digitizer to insure phase-coherent signal recovery. A block diagram of the new configuration is shown in Fig. 1. The synthesizer (a) signal at frequency ν, referenced to a 10-MHz source (b), is split into a stimulating signal path (I) (to the Fabry–Perot cavity) and a down conversion signal path (II) to the image rejection mixer (l) (*10b*). The 10-MHz reference is tripled to 30 MHz (c) to generate a frequency ν + 30 MHz in the single sideband mixer (h), which is used to tune the Fabry–Perot cavity and polarize molecules in the pulsed beam. The pulse sequencer (i), also referenced to the 10-MHz source (b), is a duplicate of the circuit developed by the Kiel group (*10a–10c*) and is controlled by a PC digital I/O interface. The pulse sequencer provides TTL pulses to control the nozzle, radio-frequency (30 MHz), and microwave switches and to trigger the digitizer. The ex-

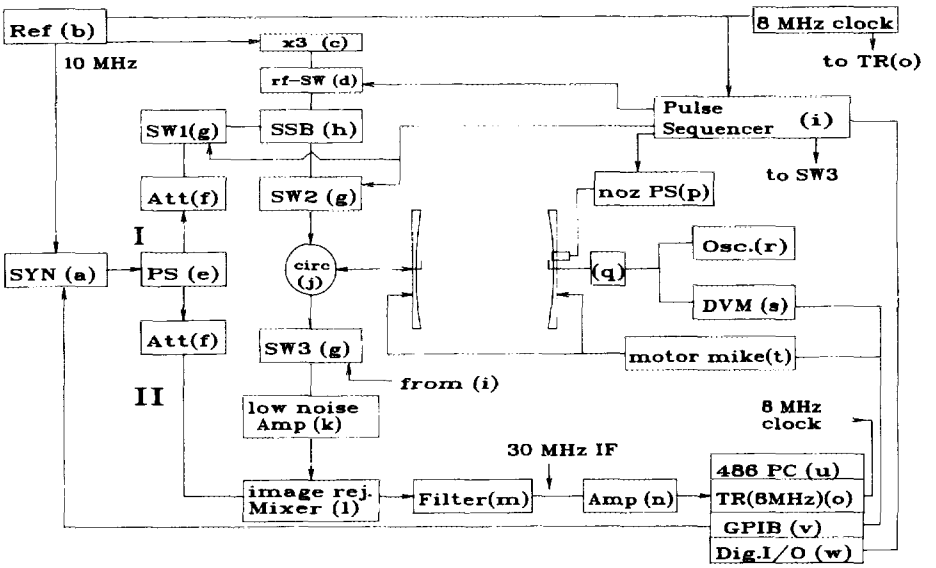

FIG. 1. Block diagram of the electronic components of the FTMW spectrometer. In the center of the diagram is shown a schematic of the mirror configuration with coupling antenna and nozzle in the mirror. The microwave configuration begins with the synthesizer (a), HP8340A/B, which is referenced to 10 MHz, Austron 1295D:1120L. Two paths are defined (I and II) by the power splitter (e). Path I follows to attenuator (f) and switch 1 (g), American Microwave SW-2184–1A, to the single sideband modulator (h), Miteq SMO 226LC1A, which is in turn fed by the times 3 multiplier of the 10 MHz signal (c), Techtrol FAX217–30, through an rf switch (d), Mini Circuits MCL ZMSW-1111. Microwave switch 2 (g) allows radiation to the circulator (j) and the cavity. The pulse sequencer (i), Ref (*10*), controls each of the pin diode switches as well as the nozzle (p), General Valve Iota One. After the beam pulse and microwave pulse radiation from the cavity is removed from the circulator (j) through switch 3 (optional) to the amplifier (k), Miteq AMF-7B-6018-37, and image rejection mixer (l), Miteq ARO526LG1A. The Intermediate frequency of 30 MHz passes through a filter (m), Reactel 6B6-30-0.6-S-11, and rf amplifier (h), Tron-Tech L30B-7, to the transient recorder board (o), Dr. Straus TRAS-25, in the PC (u). For mirror movement the motor micrometers (t), Oriel 18094, synthesizer (a), and digital volt meter (s), HP3457A, are controlled from the PC through an IEEE422 (v) interface, National Instruments (NI) GPIB-AT, with the resonance peak detected from the diode (q), Dorado CD-1-26, on the digital volt meter and oscilloscope (r). The pulse sequencer is controlled by a digital I/O board (w), NI Lab PC, synchronously with the 10 MHz reference (b). The 30 MHz signal is digitized at 8 MHz from a clock derived form the 10 MHz reference (b).

periment is initialized with digitization of a background noise spectrum and followed by a signal digitization (with the molecular-beam pulse) of the spectrum from which the noise spectrum is subtracted. The signal sequence is begun with the molecular beam pulse and after some delay, typically 0.5 msec, the radio-frequency (rf) switch (d) and microwave switches (g) are opened to generate a short microwave pulse (typically 0.5–3 μsec) to polarize molecules having a transition within the spectral bandwidth of the microwave pulse. After a delay of a few microseconds from the microwave pulse, the microwave switch (SW3 (g)) (this is an optional component to protect the detection path from high-power pulses) is opened and the digitizer is triggered; this delay is selected to eliminate any residual microwave power from the cavity energization which can cause a false signal. The signal coupled out of the cavity passes to the circulator (j), low noise amplifier, and image rejection mixer (l) (30 MHz intermediate frequency (IF)), and is then digitized in the transient recorder (o) with an 8-MHz clock derived from the 10-MHz source (b) into 4096 channels. One of the advantages

of this overall configuration is the ease of automated broadband scans (*10c*), since all of the components are controlled by the computer (u). Up to 200 MHz per hour may be covered in favorable circumstances, and the system may be unattended during this process.

In addition to the limiting bandwidth of the cavity, generally 300 kHz to several MHz, a six-stage filter (m) limits the 30-MHz IF signal to ± 300 kHz (3 dB level). Thus, the signal recovered after a Fourier transform is centered at 30 ± 0.3 MHz. Due to digitizing, the 30-MHz IF signal for the upper sideband (ν + 30 MHz) at an 8-MHz rate (chosen for full sampling of the 30-MHz signal), the effective transformed signal is centered in a window of 4 MHz (one-half of the clock frequency) determined by 30 MHz − $n\nu_{\text{clock}}$ = −2 MHz (n is a integer) for the upper sideband selected, and the frequency scale from the Fourier transform should be inverted to provide a scale increasing from left to right. The effective signal would be +2 MHz if the lower sideband (ν − 30 MHz) were chosen, i.e., −30 MHz + $n\nu_{\text{clock}}$), and no frequency inversion is necessary after the transform. As a result of the total time of digitizing, 512 μsec (0.125 μsec × 4096 channels), the resolution per channel in the frequency domain is 1.953 kHz. Because of the longer interaction time of beam and free-induction decay, signal-to-noise improvements on the transformed signal of up to a factor of 25 have been obtained with a number of van der Waals species studied previously with the earlier version of the spectrometer (*6, 7*). From the path length increase to approximately 60 cm, compared to about 10 cm with a nozzle perpendicular to the cavity axis, coupled with a longer beam pulse, we could only expect a signal-to-noise improvement of about 6. The factor of 25 improvement is realized, both due to a larger overlap between the molecular beam with the active region of the cavity and to the narrower linewidth intrinsic to an axial beam, which provides the additional S/N improvement by means of a longer lasting signal. Any effects which broaden the lines, e.g., partially resolved spin–spin and nuclear quadrupole hyperfine structure, eliminate the enhancement related to line narrowing.

III. OBSERVED SPECTRUM AND ASSIGNMENT

Our initial survey of the spectrum for nitromethane-water covered regions from 8 to 9 GHz and 9 to 18 GHz, resulting in the detection of 25 transitions which require both CH_3NO_2 and H_2O for observation. Fully and partially resolved hyperfine structure from several transitions, provided tentative assignments for a number of transitions, but predictions of additional transitions from fits to the tentatively assigned lines met with failure in confirming the assignments. One of the transitions assigned, with fair certainty, was the 1_{11}–0_{00} transition near 12 383 MHz (see Tables I and II), based on the observation of three resolved hyperfine components with splittings consistent with the value of eQq_{aa} of nitromethane (−1.184 MHz). Since this transition is *b*-type, it suggested that the *a*-axis of nitromethane lies along the *b*-axis in the complex. At this point, the higher resolution and sensitivity of the new beam configuration proved invaluable. Each transition observed in the earlier survey was reexamined, and predictions based on the quadrupole coupling constants of nitromethane (*11*) (with appropriate axes rotation) were employed in the assignments. This resulted in several reassignments, as well as several additional assignments, and the prediction of a number of new transitions which were then detected close to the predicted frequencies. After assignment of the normal isotopic species was firmly established, the isotopic variants CH_3NO_2–HDO, CH_3NO_2–D_2O, and CD_3NO_2–H_2O were studied and assigned.

TABLE I

Observed Rotational Transition Frequencies
for CH_3NO_2–H_2O and CH_3NO_2–HDO

$J'(K_-,K_+) - J''(K_-,K_+)$	F′ - F″	CH_3NO_2-H_2O /MHz	O-C[a] /kHz	CH_3NO_2-HDO /MHz	O-C[a] /kHz
2(1,2) - 1(1,1)	1 - 0	8273.851(2)	1.8	-	-
	3 - 2	8274.156(2)	0.5	-	-
	1 - 1	8274.646(2)	0.9	-	-
1(1,0) - 1(0,1)	0 - 1	8456.638(2)	1.1	8427.105(2)	2.3
	2 - 1	8457.072(2)	3.5	8427.546(2)	-5.2
	2 - 2	8457.096(2)	-3.1	-	-
	1 - 1	8457.353(2)	-3.3	8427.845(2)	2.8
2(0,2) - 1(0,1)	2 - 1	8679.716(2)	0.9	8548.924(2)	2.0
	3 - 2	8679.730(2)	0.5	8548.937(2)	-0.3
2(1,1) - 2(0,2)	1 - 1	8894.882(2)	1.7	-	-
	3 - 3	8895.004(2)	-1.6	-	-
2(1,1) - 1(1,0)	3 - 2	9117.638(2)[b]	(3.0)	-	-
4(0,4) - 3(1,3)	5 - 4	10179.077(2)	0.5	-	-
	4 - 3	10179.348(2)	-1.4	-	-
1(1,1) - 0(0,0)	1 - 1	12383.092(2)	-0.7	12296.152(2)	-1.9
	2 - 1	12383.409(2)	-2.1	12296.470(2)	-2.0
	0 - 1	12383.890(2)	1.4	12296.951(2)	1.7
3(1,3) - 2(1,2)	2 - 1	12401.078(2)	0.9	12216.763(2)	-2.2
	3 - 2	12401.129(2)	-0.4	12216.816(2)	1.0
	4 - 3	12401.137(2	-0.6	12216.829(2)	2.1
3(0,3) - 2(0,2)	3 - 2	12979.122(2)	0.3	-	-
	4 - 3	12979.147(2)	0.2	12784.413(2)[b]	-
	2 - 1	12979.157(2)	-1.9	-	-
3(2,2) - 2(2,1)	4 - 3	13043.691(2)[b]	(4.0)	-	-
3(1,2) - 2(1,1)	4 - 3	-	-	13456.883(2)	-6.5
	3 - 2	-	-	13456.904(2)	2.2
	2 - 1	-	-	13456.958(2)	2.8
5(0,5) - 4(1,4)	6 - 5	15084.585(2)[b]	(1.0)	-	-
2(1,2) - 1(0,1)	2 - 1	16309.244(2)	-6.7	16164.886(2)	5.1
	3 - 2	16309.590(2)	0.4	16165.218(2)	-2.4
	1 - 0	16309.805(2)	-1.8	-	-
4(1,4) - 3(1,3)	3 - 2	16516.517(2)	-2.0	-	-
	4 - 3	16516.535(2)	1.2	16271.473(2)[b]	-
	5 - 4	16516.548(2)	2.6	-	-
4(0,4) - 3(0,3)	4 - 3	17230.903(2)	1.2	16973.915(2)	2.4
	5 - 4	17230.936(2)	-0.4	16973.947(2)	-0.7
	3 - 2	17230.945(2)	0.6	-	-

[a] Observed-minus-calculated frequency difference.
[b] Unresolved structure, not included in the hyperfine analysis.

The spectral measurements for the four isotopomers investigated are listed in Tables I and II, and the hypothetical rotational frequencies (free of ^{14}N hyperfine structure) are listed in Table III; the uncertainties shown in parentheses are estimated to be two standard deviations and are based on the resolution element, blending, and signal-to-noise considerations. The fitted parameters are listed in Table IV for both hyperfine structure and rotation. Only the *A*-symmetry species transitions of the CH_3 internal-rotor states of CH_3NO_2–H_2O were assigned, but a few transitions were recorded which might belong to the *E*-symmetry species based on the observation of a first order Stark effect. It appears that the barrier to internal rotation is rather small, as evidenced by the large A–E transition frequency splittings from tentative assignments, and at the present time we have not succeeded in assigning most of the observed *E*-state transitions. The *A*-state transition pattern is sufficiently regular that we could apply the traditional Watson Hamiltonian (*12*) and reduce the spectrum to the constants in Table IV. The hyperfine structure analysis was derived in a similar manner to that described by Kirchhoff and Johnson (*13*), and the center frequencies were fitted to

TABLE II

Observed Rotational-Hyperfine Transition Frequencies for CH_3NO_2–D_2O and CD_3NO_2–H_2O

$J'(K_-,K_+)$ - $J''(K_-,K_+)$	F' - F''	CH_3NO_2-D_2O /MHz	O-C[a] /kHz	CD_3NO_2-H_2O /MHz	O-C[a] /kHz
2(1,2) - 1(1,1)	3 - 2	-	-	8084.820(4)[b]	-
2(0,2) - 1(0,1)	3 - 2	8152.469(2)[b]	-	8524.879(4)[b]	-
1(1,0) - 1(0,1)	2 - 2	8469.836(2)[b]	-	-	-
2(1,1) - 1(1,0)	3 - 2	-	-	9014.008(4)[b]	-
3(1,3) - 2(1,2)	3 - 2	11675.004(2)[b]	1.8	-	-
	4 - 3	11675.017(2)	-1.3	12112.031(4)[b]	-
1(1,1) - 0(0,0)	1 - 1	12175.679(2)	-2.9	10605.451(4)	1.2
	2 - 1	12176.002(2)	4.4	10605.772(4)	-0.8
	0 - 1	12176.470(2)	-1.3	10606.259(4)	1.6
3(0,3) - 2(0,2)	3 - 2	12196.542(2)	2.6	12725.936(4)	0.2
	4 - 3	12196.563(2)	-0.3	12725.972(4)	0.1
	2 - 1	12196.571(2)	1.7	-	-
3(1,2) - 2(1,1)	4 - 3	-	-	13504.878(4)[b]	-
4(1,4) - 3(1,3)	4 - 3	15552.054(2)	-0.1	-	-
	5 - 4	15552.069(2)	0.2	16122.146(4)[b]	-
2(1,2) - 1(0,1)	2 - 1	-	-	14415.461(4)	2.2
	3 - 2	15882.022(2)	0.1	14415.803(4)	-0.1
	1 - 0	15882.212(2)	-1.0	14416.017(4)	-1.3
4(0,4) - 3(0,3)	4 - 3	-	-	16856.011(4)	2.0
	5 - 4	16202.655(2)[b]	-	16856.054(4)	-3.5
	3 - 2	-	-	16856.067(4)	0.1
3(1,3) - 2(0,2)	4 - 3	-	-	18002.923(8)	-6.6
	2 - 1	-	-	18003.053(8)	5.6

[a] Observed-minus-calculated frequency difference.
[b] Unresolved structure, not included in the hyperfine analysis.

the Watson Hamiltonian (*12*) in the *A*-reduction. For the most part, we have fitted the spectra for the various isotopic species to the experimental uncertainty; however, several transitions of the deuterated species show a somewhat larger deviation due to the additional unresolved deuterium nuclear quadrupole hyperfine structure.

TABLE III

Hypothetical Hyperfine-Free Rotational Transition Frequencies

$J'(K_-,K_+)$-$J''(K_-,K_+)$	CH_3NO_2-H_2O /MHz	O-C[a] /kHz	CH_3NO_2-HDO /MHz	O-C[a] /kHz	CH_3NO_2-D_2O /MHz	O-C[a] /kHz	CD_3NO_2-H_2O /MHz	O-C[a] /kHz
2(1,2) - 1(1,1)	8274.140(2)	-3.0	-	-	-	-	8084.804(4)	3.3
1(1,0) - 1(0,1)	8457.142(2)	0.4	8427.617(2)	-3.3	8469.890(2)	-4.1	-	-
2(0,2) - 1(0,1)	8679.728(2)	1.1	8548.935(2)	-0.1	8152.464(2)	-1.4	8524.874(4)	-5.5
2(1,1) - 2(0,2)	8895.078(2)	0.0	-	-	-	-	9014.036(4)	-1.0
2(1,1) - 1(1,0)	9117.663(2)	2.7	-	-	-	-	-	-
4(0,4) - 3(1,3)	10179.144(2)	-2.3	-	-	-	-	-	-
1(1,1) - 0(0,0)	12383.358(2)	-2.9	12296.419(2)	2.4	12175.945(2)	1.3	10605.719(4)	-1.2
3(1,3) - 2(1,2)	12401.128(2)	1.7	12216.815(2)	-4.7	11675.005(2)	0.1	12112.020(4)	3.6
3(0,3) - 2(0,2)	12979.141(2)	2.7	12784.408(2)	1.1	12196.557(2)	1.8	12725.963(4)	-2.4
3(2,2) - 2(2,1)	13043.694(2)	-0.3	-	-	-	-	-	-
3(1,2) - 2(1,1)	-	-	13456.902(2)	0.9	-	-	13504.990(4)	0.6
5(0,5) - 4(1,4)	15084.649(2)	-0.1	-	-	-	-	-	-
2(1,2) - 1(0,1)	16309.516(2)	-2.0	16165.146(2)	0.9	15881.947(4)	-6.9	14415.728(4)	10.0
4(1,4) - 3(1,3)	16516.536(2)	-1.3	16271.464(2)	2.4	15552.059(2)	0.5	16122.136(4)	1.7
4(0,4) - 3(0,3)	17230.927(2)	2.6	16973.938(2)	-1.4	16202.646(2)	-2.3	16856.044(4)	0.4
3(1,3) - 2(0,2)	-	-	-	-	-	-	18002.846(4)	-8.9

[a] Observed-minus-calculated frequency difference.

TABLE IV

Rotational and Nuclear Electric Quadrupole Coupling Constants for Isotopic Species of the Nitromethane–Water Complex[a]

Parameter	CH_3NO_2-H_2O	CH_3NO_2-HDO	CH_3NO_2-D_2O	CD_3NO_2-H_2O
A	10420.253(5)[b]	10362.026(6)[b]	10322.915(5)[b]	8700.694(14)[b]
B	2384.882(4)	2347.905(5)	2229.635(9)	2369.726(7)
C	1963.115(2)	1934.402(3)	1856.057(9)	1905.091(5)
Δ_J	0.00307(6)	0.00278(9)	0.00253(8)	0.00336(13)
Δ_{JK}	-0.00144(42)	0.0019(12)	0.011(5)	0.0266(16)
δ_J	0.00026(7)	0.00027(10)	0.00018(9)	0.00052(15)
Δ^c /u·Å^2	-2.972	-2.760	-2.894	-6.071
eQq_{aa} (^{14}N)	0.102(5)	0.065(11)	0.012(17)	0.085(25)
eQq_{bb} (^{14}N)	-1.061(4)	-1.061(8)	-1.053(7)	-1.077(9)
eQq_{cc} (^{14}N)	0.959(5)	0.997(10)	1.041(20)	0.992(29)
σ^d	1.1	1.0	0.6	1.7

[a] The values are given in MHz with the exception of the inertial defect, Δ.

[b] Uncertainties shown in parentheses refer to the least significant digit(s) and are two standard deviation.

[c] Inertial defect, $\Delta = I_c - I_a - I_b$, in u·Å.

[d] Unitless standard deviation of the weighted least-squares fit.

Noteworthy is the inertial defect, $\Delta = I_c - I_a - I_b$, among the various isotopomers which is listed in Table IV. These values are close to what one expects for a hindered rotor CH_3 or CD_3, −3.27 and −6.52 u·Å^2, respectively. The invariability of the inertial defects for the species containing CH_3NO_2 indicates that the water molecule lies in the heavy atom plane of the nitromethane unit. Also note that the value eQq_{bb} = −1.061 MHz of the complex is nearly equal to the value eQq_{aa} = −1.184 MHz of nitromethane, indicating that the line joining the centers of masses of the two monomers is nearly perpendicular to the C–N bond of nitromethane.

IV. STRUCTURE

The usual assumption was made in determining the structure of the dimer, namely, that the structure of the monomer units are unchanged upon complex formation. With this assumption and the further observation that the water oxygen atom lies in the heavy atom plane of the complex, there only remains to be determined the center of mass separation, R_{cm}, two angles, θ and ϕ, which define the angular orientation of each unit with respect to R_{cm}, and a rotation angle, γ, about the symmetry axis of nitromethane, i.e., out of plane rotation of the NO_2 group, as defined in Fig. 2. The fixed structural values for nitromethane, taken from the substitution structure of Cox and Waring (*14*), are r(CN) = 1.489 Å, r(NO) = 1.224 Å, r(CH) = 1.088 Å, ∠HCH = 107.2°, and ∠ONO = 125.3°, and the values for water are r(HO) = 0.9565 Å and ∠HOH = 105.0° from a structural fit of the H_2O, HDO, and D_2O species. In principle, a rotation of the H_2O entity about its symmetry axis should also be considered; however, we find that this rotation gives larger standard deviations when fixed at nonzero values.

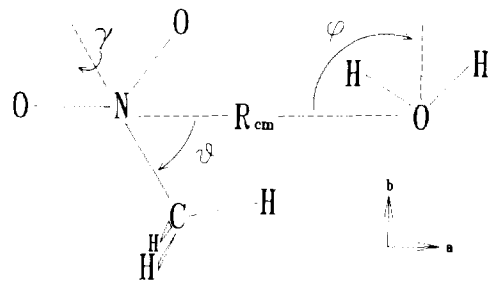

FIG. 2. Definition of the structural parameters of CH_3NO_2–H_2O.

The initial fits assumed the complex to be planar, with the exception of the CH_3 group. When all three moments of inertia for the four observed isotopic forms were least-squares fitted to three parameters, R_{cm}, θ, and ϕ, a rather poor fit was obtained with $\sigma = 1.6$ u · Å^2. This poor fit may result from the relatively low barrier to internal rotation of the methyl group, which should affect the I_b moment the most since the internal rotation angular momentum is along this axis. In nitromethane the CH_3 (or CD_3) group is nearly a free rotor with internal rotation angular momentum along the a-axis, the protons (or deuterons) do not contribute to the I_a moment of inertia (*14*). Next, the moments of inertia, I_a and I_c, for the four isotopic species were fit to three structure parameters (again assuming planarity of the heavy atoms) with a resulting standard deviation (σ) of 0.85 u · Å^2. Actually, two equivalent fits were obtained in each case. In both fits the b-axis of water is approximately parallel to the a-axis of nitromethane, and in the first fit the hydrogen atoms of water are located in the same direction as the oxygen atoms of NO_2 (monomer dipoles opposed), while in the second fit the hydrogen atoms of water are directed toward the methyl group (monomer dipoles aligned). This second form seems quite unlikely since the negatively charged atoms are adjacent and the positively charged protons are adjacent. The measurement of the dipole moment described in the next section eliminates this structure from further consideration. The structure values obtained in the first case described above are $R_{cm} = 3.483(6)$ Å, $\theta = 75(4)°$, and $\phi = 99(11)°$ with a standard deviation of 0.84 u · Å^2, and are listed as Fit I in Table V (one standard deviation uncertainties are shown in parentheses, here, and later in this section). While this fit represents an improvement over the fit to three moments of inertia, it still has a rather large standard deviation. A final fit (labeled Fit II in Table V) was carried out with four variables, the three original parameters plus the rotation angle, γ, of the NO_2 group, again with only I_a and I_c moment data. This analysis converged with a value of γ near 15° and a standard deviation of 0.42 u · Å^2, a factor of 2 improvement over the planar fit. The final values for Fit II are $R_{cm} = 3.506(7)$ Å, $\theta = 63.9(32)°$, $\phi = 86(6)°$, and $\gamma = 14.6(24)°$, and the resulting structure is shown in Fig. 3.

V. DIPOLE MOMENT DETERMINATION

Stark effect measurements were carried out on many of the nitromethane–water transitions, but only a few provided rather well resolved components, and these were used in the analysis of the dipole moment. Since the Stark shifts are comparable to the hyperfine energy splittings, the analysis required a Stark-hyperfine Hamiltonian

TABLE V

Molecular Structure Fit Results

Parameter	Fit I planar[a]	Fit II non-planar[a,b]	
R_{cm} /Å	3.483(6)[c]	3.506(7)[c]	
θ /degrees	75(4)	63.9(32)	
ϕ /degrees	99(11)	86(6)	
γ /degrees	0	14.6(24)	
σ /u·Å^{2d}	0.84	0.42	
Derived Values			Experiment
$r(O_{nitro}$-$H_{water})$ /Å	1.97(12)	2.16(7)	
$r(O_{water}$-$H_{methyl})$ /Å	2.40(14)	2.09(10)	
μ_a /10^{-30} C·m	4.04 (1.21 D)	4.60 (1.38 D)	4.15 (1.423 D)
μ_b /10^{-30} C·m	4.67 (1.40 D)	3.97 (1.19 D)	5.96 (1.706 D)

[a] Water protons in the same direction as the NO_2 group.

[b] The NO_2 group is rotated out of plane about its symmetry axis by γ.

[c] Uncertainties shown in parentheses are one standard deviation.

[d] Standard deviation of the fit.

which treated the intermediate field case. The configuration and calibration of the Stark field with the $J = 1$–0 line of OCS has been described in many prior reports(*3–5, 7*). Stark shifts up to 300 kHz were measured for the 1_{11}–0_{00}, 2_{12}–1_{01}, 3_{03}–2_{02}, and 3_{12}–2_{11} transitions. Least-squares analysis of 27 shifted components for these lines provides the dipole moment values of $\mu_a = 4.15(4) \times 10^{\times 30}$ C·m [1.243(11) D] and $\mu_b = 5.69(4) \times 10^{\times 30}$ C·m [1.706(12) D]. In these fits no evidence is found for a nonzero value for μ_c. The dipole moment analysis can rule out the co-aligned geometry of the complexes. Assuming no induced dipole moment, the vector addition of the monomer dipole moments for the structure fits are shown in Table V for anti-alignment of the monomer dipole moments. For the case of the structural form with dipoles aligned, discussed in the previous section, the projected dipole moment components are $\mu_a = 4.24 \times 10^{-30}$ C·m [1.27 D] and

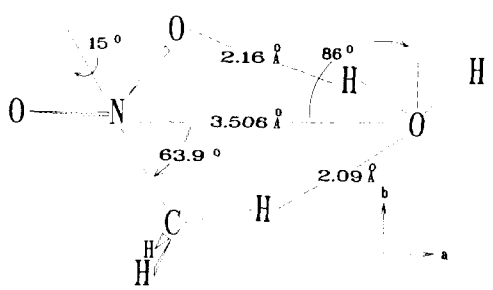

FIG. 3. Experimentally determined structure of the nitromethane–water complex from Fit II of Table V.

TABLE VI

Comparison of Force Constants, k_S, and van der Waals Stretching Frequencies, ω_S, for Several Dimers Exhibiting Large Values

Species	k_s /Nm^{-1}	ω_s /cm^{-1}	R_{cm} /Å	Ref.
CH_3NO_2-H_2O	9.3	106.6	3.506(7)	present
$(H_2O)_2$	10.8	143	2.98	a
H_2CO-HF	8.8	110	2.874	b
$(H_2CO)_2$	6.2	84	3.05	c
H_2O-SO_2	7.7	96	2.96	d
CH_3CN-BF_3	9.4	79	3.411	e
NH_3-HCN	12.2	141	3.8466	f
$(CH_3)_3N$-HCN	14.7	116.1	4.007	g

[a]Ref. 16 [b]Ref. 17 [c]Ref. 18 [d]Ref. 19 [e]Ref. 20 [f]Ref. 21 [g]Ref. 22

$\mu_b = 17.2 \times 10^{-30}$ C · m [5.15 D]. Clearly only the antialigned structures of Fits I and II are consistent with the experimentally determined values.

VII. DISCUSSION

Structural information is also available from the measured nuclear electric quadrupole coupling constants of the nitromethane–water complex. The coupling constants for the complex are determined from the vibrationally averaged projections of the coupling constants of nitromethane onto the inertial axes of the complex, assuming that the electric field gradient at the nitrogen nucleus is unaffected by complex formation. The diagonal components of the quadrupole tensor of nitromethane have been determined by Cox and Waring (*11*) and are $\chi_{aa} = -1.184(7)$ MHz, $\chi_{bb} = 0.305(12)$ MHz, and $\chi_{cc} = 0.880(12)$ MHz, where $\chi_{xx} = eQq_{xx}$. By using the rotation matrix which converts the inertial tensors in the nitromethane frame to that of the complex in Fits I and II of Table V, we obtain $\chi_{aa} = 0.189(11)$ MHz and $\chi_{bb} = -1.068(7)$ MHz for the planar form (Fit I), and $\chi_{aa} = 0.011$ MHz and $\xi_{bb} = -0.861(6)$ MHz for the nonplanar form (Fit II). Comparison of these values with the observed values in Table IV indicates closer agreement with the planar fit, while the nonplanar fit to the moments of inertia provides the lower standard deviation. The structure shown in Fig. 3 from Fit II (nonplanar form) is very similar to the transition state structure reported by Melius (*2*) and suggests that this hydrogen bonded structure lies along the reaction coordinate for the conversion of nitromethane to it *aci* version $CH_2N(O)OH$.

By most measures nitromethane–water is a very strongly bonded dimer. It exhibits rather compact dual hydrogen bond distances, i.e., 2.1 Å, and a fairly large van der Waals stretching force constant. The pseudodiatomic force constant (*15*) for the van der Waals stretch is derived from R_{cm} and Δ_J,

$$k_s = 16\,\pi^4\,\mu_D^2 R_{cm}^2\,[4B_D^2 + 4C_D^2 - (B_D - C_D)^2\,(B_D + C_D)^2]/hD_J, \qquad (2)$$

with the resulting value $k_s = 9.30$ N · m^{-1}, corresponding to a stretching frequency of $\omega_s = 106.6$ cm^{-1}. Comparison of these values with other hydrogen bonded and

van der Waals species is provided in Table VI. From this comparison it is clear that nitromethane–water is one of the stronger-bonded species in these classes of dimers.

ACKNOWLEDGMENTS

This work was supported in part by the U.S. Army Research Office. The authors are grateful to H. Dreizler for providing the pulse sequencer circuit, and to W. J. Stevens for discussions of the structure of the dimer.

RECEIVED: November 9, 1994

REFERENCES

1. C. F. MELIUS, *in* "Chemistry and Physics of Energetic Materials" (S. Bulusu Ed.), NATO Adv. Sci. Inst. Ser. E: Appl. Sci., Kluwer, Dordrecht.
2. C. A. MELIUS, *Philos. Trans. R. Soc. London A* **339,** 365–376 (1992).
3. J. Z. GILLIES, C. W. GILLIES, R. D. SUENRAM, F. J. LOVAS, AND W. STAHL, *J. Am. Chem. Soc.* **111,** 3073–3074 (1989); C. W. GILLIES, J. Z. GILLIES, R. D. SUENRAM, F. J. LOVAS, E. KRAKA, AND D. CREMER, *J. Am. Chem. Soc.* **113,** 2412–2421 (1991).
4. J. Z. GILLIES, C. W. GILLIES, F. J. LOVAS, K. MATSUMURA, R. D. SUENRAM, E. KRAKA, AND D. CREMER, *J. Am. Chem. Soc.* **113,** 6408–6415 (1991).
5. C. W. GILLIES, J.Z. GILLIES, F.J. LOVAS, AND R.D. SUENRAM, *J. Am. Chem. Soc.* **115,** 9253–9262 (1993).
6. F. J. LOVAS AND R. D. SUENRAM, *J. Chem. Phys.* **87,** 2010–2020 (1987).
7. R. D. SUENRAM, F. J. LOVAS, G. T. FRASER, J. Z. GILLIES, C. W. GILLIES, AND M. ONDA, *J. Mol. Spectrosc.* **137,** 127–137 (1989).
8. T. J. BALLE AND W. H. FLYGARE, *Rev. Sci. Instrum.* **52,** 33–45 (1981).
9. J.-U. GRABOW AND W. STAHL, *Z. Naturforsch. A* **45,** 1043–1044 (1990).
10. (a) U. ANDRESEN, private communication; (b) J.-U. GRABOW, PH.D. Thesis, Universität Kiel, (1992); (c) U. ANDRESEN, H. DREIZLER, J.-U. GRABOW, AND W. STAHL, *Rev. Sci. Instrum.* **61,** 3694–3699 (1990).
11. A. P. COX, S. WARING, AND K. MORGENSTERN, *Nature Phys. Sci.* **229,** 22–23 (1971).
12. J. K. G. WATSON, *in* "Vibrational Spectra and Structure, A Series of Advances" (J. R. Durig, Ed.), Vol. 6, pp. 1–89, Elsevier, New York/Amsterdam, 1977.
13. W. H. KIRCHHOFF AND D. R. JOHNSON, *J. Mol. Spectrosc.* **45,** 159–165 (1973).
14. A. P. COX AND S. WARING, *Faraday Trans. 2* **68,** 1060–1071 (1972).
15. D. J. MILLEN, *Can. J. Chem.* **63,** 1477–1479 (1985).
16. T. R. DYKE, K. M. MACK, AND J. S. MUENTER, *J. Chem. Phys.* **66,** 498–510 (1977).
17. F. A. BAIOCCHI AND W. KLEMPERER, *J. Chem. Phys.* **78,** 3509–3520 (1983).
18. F. J. LOVAS, R. D. SUENRAM, L. H. COUDERT, T. A. BLAKE, K. J. GRANT, AND S. E. NOVICK, *J. Chem. Phys.* **92,** 891–898 (1990).
19. K. MATSUMURA, F. J. LOVAS, AND R. D. SUENRAM, *J. Chem. Phys.* **91,** 5887–5894 (1989).
20. M. DVORAK, R. S. FORD, R. D. SUENRAM, F. J. LOVAS, AND K. R. LEOPOLD, *J. Am. Chem. Soc.* **114,** 108–115 (1992).
21. G. T. FRASER, K. R. LEOPOLD, D. D. NELSON, JR., A. TUNG, AND W. KLEMPERER, *J. Chem. Phys.* **80,** 3073–3077 (1984).
22. C. A. REGO, R. C. BATTEN, AND A. C. LEGON, *J. Chem. Phys.* **89,** 696–702 (1988).